Granular Matter (2006) 8: 175–184
DOI 10.1007/s10035-006-0013-3

ORIGINAL PAPER

Andrew C. Collop · Glenn R. McDowell · York W. Lee

Modelling dilation in an idealised asphalt mixture using discrete element modelling

Received: 12 September 2005 / Published online: 21 April 2006

Abstract This paper investigates the use of discrete element modelling (DEM) to simulate the behaviour of a highly idealised bituminous mixture under uniaxial and triaxial compressive creep tests. The idealised mixture comprises single-sized spherical (sand-sized) particles mixed with bitumen and was chosen so that the packing characteristics are known (dense random packing) and the behaviour of the mixture will be dominated by the bitumen and complex aggregate interlock effects will be minimised. In this type of approach the effect of the bitumen is represented as shear and normal contact stiffnesses. A numerical sample preparation procedure has been developed to ensure that the final specimen is isotropic and has the correct volumetrics. Elastic contact properties have been used to investigate the effect of the shear and normal contact stiffnesses on bulk material properties. The bulk modulus was found to be linearly dependent on the normal contact stiffness and independent of the shear contact stiffness. Poisson's ratio was found to be dependent on only the ratio of the shear contact stiffness to the normal contact stiffness. An elastic contact has been assumed for the compressive normal contact stiffness and a viscoelastic contact for shear and tensile normal contact stiffness to represent the contact behaviour in idealised mixture. The idealised mixture is found to dilate when the ratio of compressive to tensile contact stiffness increases as a function of loading time. Uniaxial and triaxial viscoelastic simulations have been performed to investigate the effect of stress ratio on the rate of dilation with shear strain for the sand asphalt. The numerical results have been validated with experimental data.

Keywords Asphalt · Elastic · Viscoelastic · Uniaxial · Triaxial · Creep · Discrete element modelling · Dilation

A.C. Collop (✉) · Y.W. Lee
Nottingham Centre for Pavement Engineering,
University of Nottingham, University Park,
Nottingham NG7 2RD, UK
E-mail: andrew.collop@nottingham.ac.uk
E-mail: evxywl@nottingham.ac.uk
Tel.: +44-115-9513935
Fax: +44-115-9513898

G.R. McDowell
Nottingham Centre for Geomechanics,
University of Nottingham, University Park,
Nottingham NG7 2RD, UK
E-mail: glenn.mcdowell@nottingham.ac.uk
Tel.: +44-115-9514603
Fax: +44-115-9513898

1 Introduction

Asphalt is a complex multi-phase material comprising mineral aggregate, filler, bitumen and air. A range of asphalt mixtures can be produced depending on the proportions of these components and the grading of aggregate. A typical continuously graded mixture (e.g. asphalt concrete) relies on an interlocking aggregate skeleton for its strength with the binder primarily acting as a lubricant to aid compaction and "glue" the mixture together. At the other extreme, a typical gap-graded mixture (e.g. stone mastic asphalt, SMA) will have a discontinuous aggregate grading (i.e. some stone sizes will not be present) and relies on a coarse aggregate skeleton bound by a bitumen/filler "mortar" for its strength. For both these mixture types the micromechanical behaviour, at the scale of an aggregate particle, is an important factor in terms of overall material performance.

For example, it has been found that the aggregate structure has a profound influence on the resistance to permanent deformation of an asphalt mixture with different laboratory compaction methods producing very different permanent deformation characteristics [1–3]. Sousa et al. [3] compared the permanent deformation behaviour of well compacted field and laboratory specimens using the same mixture and the same air void content. They found that kneading compaction resulted in a stronger aggregate structure than that found in the field cores, rolling wheel compaction resulted in a structure approximately the same as in the field, and gyratory compaction resulted in a much weaker structure. Other researchers have found similar results [4–6] and it is clear that the aggregate orientation and the effect of this internal structure on the volumetrics, permeability and mechanical proper-

ties of the compacted materials, is important in determining the mechanical properties of the mixture.

The traditional approach to modelling asphaltic materials is to treat them at the macro-scale using continuum-based models [7]. This usually involves undertaking careful experiments over a range of conditions (e.g. stress levels, loading rates, temperatures etc), measuring the macroscopic response of the material and fitting continuum-based constitutive models (which can be extremely complex) to the measured behaviour. The micromechanical behaviour of the mixture is not explicitly included in this approach which means that it is not easy to relate observed behaviour to the micromechanics of the material.

2 Discrete element modelling

Discrete element modelling (DEM) for granular assemblies was developed by Cundall and Strack [8]. In their original BALL model, no bonding of particles was permitted. The software used in this research, PFC3D Version 3 [9], permits bonding of particles and user-defined contact models. PFC3D models the movement and interaction of assemblies of rigid spherical particles subjected to external stresses. The particles displace independently from each other and interact only at point contacts. A finite stiffness is taken to represent the measurable stiffness that exists at a contact. The program uses the so called "soft contact approach" whereby the particles are assumed to be rigid but they are allowed to overlap each other at the contact points (the overlap is assumed to be small compared to the particle size). The magnitude of the overlap is related to the contact force via a force–displacement law. The mechanical behaviour of the system is described in terms of the movement of each particle and the inter-particle forces which are related using Newton's laws of motion.

PFC3D allows particles to be bonded together at contact points such that, when a pre-defined bond strength is reached, the bond is broken. Although the particles are spherical, super-particles of arbitrary shape can be created which comprise a set of overlapping particles (clump) that act as a rigid body with a deformable boundary or bonded particles which act as a deformable friable agglomerate. Typical parameters which need to be defined are the particle normal and shear stiffnesses k_n, k_s and bond strengths b_n, b_s, the particle coefficient of friction μ_b, and the platen coefficient of friction μ. The stiffness at a contact is calculated assuming that the stiffnesses of the two contacting particles act in series, and the coefficient of friction at a contact is assumed to be the lesser of the coefficients of friction of the contacting objects. In this paper the bond strengths (b_n, b_s) are taken to be large so that there is no bond breakage and the coefficients of friction (μ_b, μ) are taken to be zero to ensure that uniform uniaxial and triaxial stress conditions are generated in the numerical samples. It should be noted that the tue coefficient of friction between sand particles is significantly greater than zero. However, no bond breakage was allowed and hence frictional inter-particle behaviour was not included in the simulations. The latest version of PFC3D also permits the user to define their own contact constitutive laws. A full description of PFC3D is beyond the scope of this paper and can be found in [9].

Although DEM has been applied to model the behaviour of soils and granular materials [8,10–13], it has not been widely used to investigate the mechanical behaviour of asphaltic materials. Rothenburg et al. [14] modelled asphalt as a set of plane (two-dimensional) elastic angular particles separated by a viscoelastic bitumen. Simulations showed that the peak unconfined compressive strength was obtained when the proportion of cohesive contacts was approximately 60% and the proportion of frictional contacts was approximately 40%. Simulations of creep tests showed that the steady-state properties were also largely controlled by the proportion of frictional inter granular contacts compared to the proportion of cohesive contacts. However, the simulations were two-dimensional and no calibration with laboratory data was given.

Buttlar and You [15] used DEM to develop a two-dimensional model of an indirect tensile (IDT) test comprising 130 cylindrical stones (12.5 mm in diameter) arranged in a hexagonal packing structure glued together with asphalt mastic. They validated predictions with experimental data (for the same idealised mixture) obtaining good agreement. Buttlar and You [15] extended this approach to develop a two-dimensional IDT model of SMA using a microfabric approach whereby the various material phases are modelled as clusters of discrete elements. The aggregate structure was captured using a high-resolution optical scanner. Predicted horizontal displacements were approximately 40% greater than measurements; this was attributed to the two-dimensional microstructural representation underestimating the actual amount of aggregate interlock.

This paper investigates the use of PFC3D to simulate the behaviour of a highly idealised bituminous mixture under uniaxial and triaxial compressive creep loading. The idealised mixture comprises single-sized spherical (sand-sized) particles mixed with bitumen. The principal reasons that this form of idealised asphalt was chosen are that the packing characteristics are known (dense random packing) and the behaviour of the mixture will be dominated by the bitumen and complex aggregate interlock effects will be minimised. In this type of approach the effect of the bitumen is represented by the shear and normal contact stiffnesses.

3 Numerical sample preparation procedure

Since the objective of this paper is to simulate simple laboratory tests using DEM, it is necessary to artificially generate a test specimen that replicates an idealised asphalt mixture. It is important that the sample is initially isotropic and exhibits approximately the same packing characteristics as the idealised mixture (i.e. the same volumetrics). The following numerical specimen preparation procedure has been adopted

to prepare cylindrical samples of known dimensions containing single-sized spherical particles of known radius:

1. The approximate number of spherical particles required to give the volume of aggregate in the sample is calculated.
2. Boundaries are generated that enclose the required space and the number of particles calculated above are generated randomly inside the space.
3. The sample is allowed to cycle to equilibrium under zero external displacement so that the particles can re-orient themselves until the stresses on the sample are approximately isotropic.
4. The radii of the particles is reduced slightly (typically by less than 3%) until the isotropic stress is low (i.e. less than 1 kPa).
5. Particles with less than four contacts are detected (typically 5–8% of the total number of particles) and are expanded slightly (typically by 1%) to create additional contacts with neighbouring particles.
6. Normal and shear contact bonds are applied at each contact point.
7. The cylindrical boundary is removed and the specimen is ready for numerical testing.

Figure 1 shows a sample that has been prepared in this way containing 6,000 particles that are 1.8 mm in diameter. The specimen is 26 mm in diameter and 52 mm in length. The average number of contacts per particle for the sample shown in Figure 1 is 5.8 and the particles occupy 63.5% of the total volume. A detailed description of the effects of sample size on macroscopic material properties can be found in Collop et al. [16]. It should be noted that predictions will be compared to experimental data for an idealised sand asphalt where the sand particles are between 1.18 and 2.36 mm and occupy approximately 65% of the material volume [17].

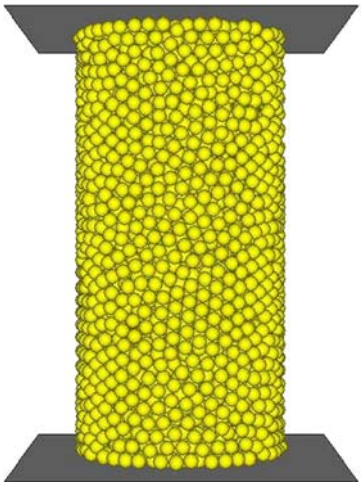

Fig. 1 Numerical sample prior to testing

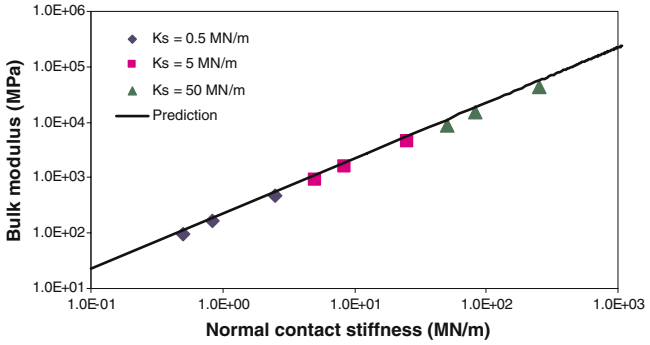

Fig. 2 Effect of normal and shear contact stiffnesses on bulk modulus

4 Elastic simulation

It was noted above that the response of this type of idealised mixture will be dominated by the bitumen. It is well known that bitumen is a material whose response depends on loading time and temperature. This section investigates the elastic part of the response by using elastic normal and shear contact stiffnesses. Time dependent effects will be introduced in a later section.

To simulate a uniaxial compressive creep test it is necessary to apply an axial load (stress) to the sample and measure the axial displacement (strain) and radial displacement (strain) during the test. The load was applied at a maximum velocity of 0.1 m/s to ensure that dynamic wave propagation effects within the sample are avoided.

4.1 Compressive contact stiffness = tensile contact stiffness

The objective of this sub-section is to investigate how the bulk material properties depend on the shear and normal contact stiffnesses where tensile and compressive normal contact stiffnesses have been taken to be equal. In these simulations, samples containing 6,000 particles were used. Results have been presented in terms of bulk modulus and Poisson's ratio to simplify the analysis and, in all cases, the compressive and tensile contact stiffnesses were taken to be equal.

Figure 2 shows a plot of bulk modulus versus normal contact stiffness for a range of shear contact stiffnesses. It can be seen from this figure that the bulk modulus is linearly related to the normal contact stiffness and is independent of the shear contact stiffness. This has been modelled using a mean field approach (see Collop et al. [16] for further details) which results in a closed form relationship between bulk modulus and normal contact stiffness that is shown by the solid line in Figure 2.

Figure 3 shows the relationship between Poisson's ratio and the ratio of shear to normal contact stiffnesses for a range of shear contact stiffnesses. It can be seen from this figure that as the ratio of shear to normal contact stiffness is increased, Poisson's ratio tends to decrease. It can also be seen from this figure that Poisson's ratio is only dependent on the ratio of shear to normal contact stiffness. This is the expected result

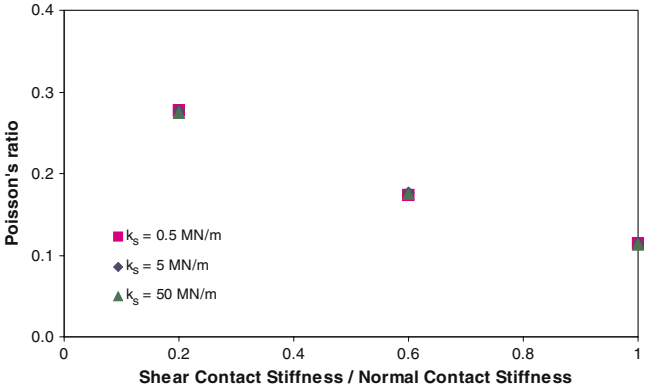

Fig. 3 Effect of normal and shear contact stiffnesses on Poisson's ratio

since, by dimensional analysis, Poisson's ratio can only depend on the ratio of contact stiffnesses and not their absolute values. It should be noted that all the values of Poisson's ratio shown in Figure 3 are less that 0.5 which indicates that the sample is reducing in volume (contracting).

5 Compressive contact stiffness ≠ tensile contact stiffness

The objective of this sub-section is to investigate the effect of non-equal tensile and compressive normal contact stiffnesses. For all simulations in this sub-section, the compressive contact stiffness is taken to be equal to 0.6 MN/m and the tensile contact stiffnesses have been reduced so that the ratio of compressive to tensile contact stiffness range from 1 to 200. Two cases have been considered; (1) the shear contact stiffness is equal to the compressive contact stiffness or (2) the shear contact stiffness is equal to the tensile contact stiffness. Figure 4 shows the dilation gradient plotted as a function of the ratio of compressive to tensile contact stiffness for the first case where the shear contact stiffness has been taken to be equal to the compressive contact stiffness. The dilation gradient (s) is defined as the tangent ratio of the volumetric strain rate ($\dot{H}$) divided by the distortional strain rate ($\dot{E}$) and has been used to quantify dilation because Poisson's ratio has no meaning for values in excess of 0.5. The volumetric strain rate ($\dot{H}$) and distortional strain rate ($\dot{E}$) are defined for a cylindrical specimen as:

$$\begin{aligned} \dot{H} &= 2\dot{\varepsilon}_{11} + \dot{\varepsilon}_{33}, \\ \dot{E} &= \dot{\varepsilon}_{33} - \frac{\dot{H}}{3} = \tfrac{2}{3}(\dot{\varepsilon}_{33} - \dot{\varepsilon}_{11}), \end{aligned} \tag{1}$$

where ε_{11} is defined as the radial strain and ε_{33} is defined as the axial strain. It should be noted that, using this sign convention for a compression test, the radial strain is tensile and positive and hence the distortional strain is negative since the axial strain is compressive and negative. In all the figures presented in this paper, the magnitude of the distortional strain has been plotted.

A negative value of dilation gradient implies that the material is reducing in volume (contracting) whereas a positive dilation gradient means that the material is increasing

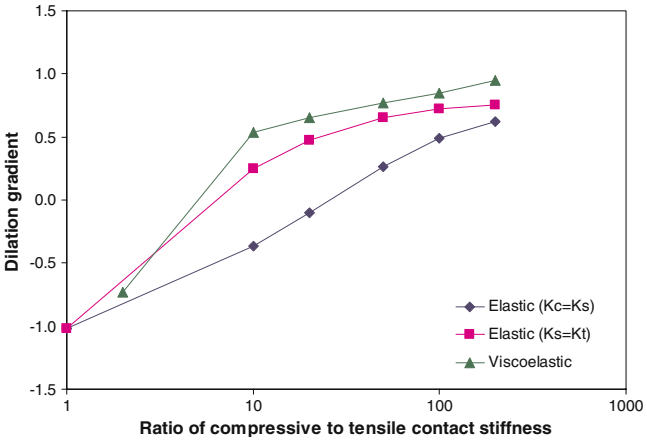

Fig. 4 Effect of the ratio of contact stiffnesses on dilation gradients

in volume (dilating). It can be seen from Figure 4 that the general trend is for the dilation gradient to increase tending towards an approximately constant value of 0.7 at high stiffness ratios indicating a significant amount of dilation which was not found when the tensile and compressive contact stiffnesses are taken to be equal (see Figure 3). This is because the relatively high compressive contact stiffnesses (compared to the tensile contact stiffness) are forcing the particles to roll past each other rather than simply overlap in compression resulting in dilation.

Also shown in Figure 4 are the corresponding results for the second case where the shear contact stiffness has been taken to be equal to the tensile contact stiffness. It can be seen that the general shape of the curve is the same as shown previously although, for the same ratio of K_C to K_T, the value of dilation gradient is greater. This is because for a given ratio of compressive to tensile contact stiffness, a lower shear contact stiffness permits higher levels of dilation at a given shear strain.

6 Viscoelastic simulations

As noted earlier, a viscoelastic model is required to capture the time dependent behaviour of bitumen. The simplest option is to use a Burger's model to represent the contact stiffnesses. A Burger's model (for the shear contact stiffness) is shown in Figure 5. It can be seen that this model comprises a spring (K_1^s) and dashpot (C_1^s) in parallel (delayed elastic component) connected in series to a spring (K_0^s, elastic

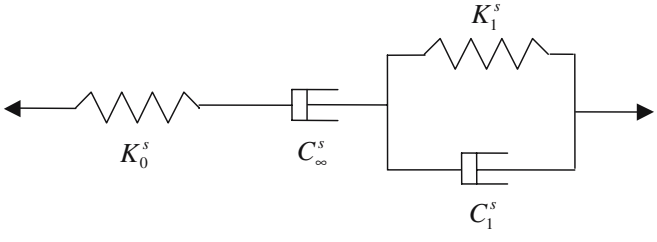

Fig. 5 Burger's viscoelastic model

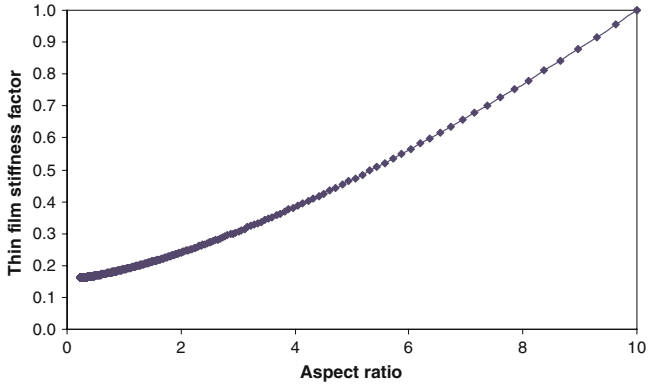

Fig. 6 The dependence of thin film stiffness factor on aspect ratio [19]

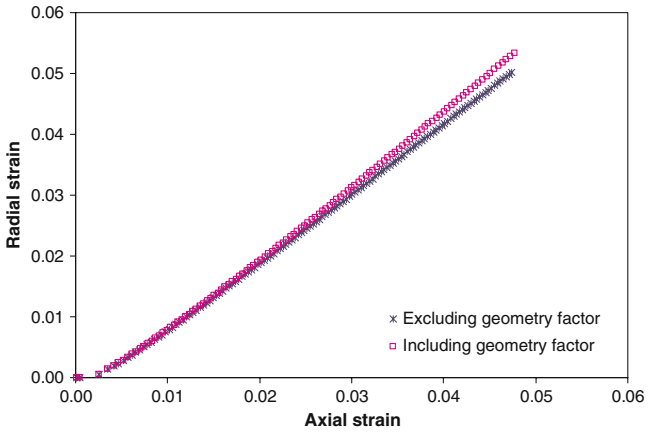

Fig. 7 The effect of thin film geometry factor in the viscoelastic simulation

component) and a dashpot (C^{s}_{∞}, viscous component). It can readily be shown that the time dependent shear stiffness of the Burger's model is given by:

$$k_s = \left[\frac{1}{K^s_0} + \frac{t}{C^s_\infty} + \frac{1}{K^s_1}\left(1 - e^{\frac{-t}{\tau^s}}\right)\right]^{-1}, \quad (2)$$

where t is the loading time and $\tau^s = C^s_1 / K^s_1$ is the relaxation time. It can be seen from equation (2) that the contact stiffness will reduce as a function of loading time. Whilst this is a reasonable approximation for the shear and normal tensile contact stiffnesses where particles are essentially moving away from each other, the normal compressive contact stiffness should increase as particles move towards each other tending towards the contact stiffness resulting from direct contact between two particles. Consequently, as a first approximation, elastic behaviour has been assumed for the compressive normal contact stiffness whereas viscoelastic behaviour has been assumed for the tensile normal contact stiffness and the shear contact stiffness.

6.1 Bitumen film geometry

Results from previous studies [18,19] have shown that the stiffness of a thin film of bitumen depends on the geometry of the film. For example, a thicker film was found to be less stiff compared to a thinner film. This section investigates the importance of this "geometric factor" on the predicted behaviour of sand asphalt mixtures.

Assuming that a thin film between two sand particles can be characterised as a disc of thickness 2 T and diameter d, where d is the diameter of the aggregate particle, the aspect ratio is given by d/T. Assuming that bitumen is incompressible, it can readily be shown that the aspect ratio is inversely proportional to the film thickness raised to the power of 3/2 (i.e. $A \propto 1/T^{3/2}$). Consequently, provided the distance between particles is known during the simulation, the aspect ratio of the bitumen films between particles can be updated using the following equation:

$$A_{t+\Delta t} = A_t \left[\frac{T}{T + \Delta U/2}\right]^{\frac{3}{2}}, \quad (3)$$

where $A_{t+\Delta t}$ is the aspect ratio at time $t + \Delta t$, A_t is the aspect ratio at time t and $\Delta\ U$ is the change in normal displacement.

During the simulation, equation (3) is used to update the "effective" aspect ratio at each contact and Figure 6 [19] is used to determine a "geometric factor" to reduce the stiffness in tension as the aspect ratio decreases. An initial aspect ratio of approximately 10 was used in equation (3) which was determined using a bitumen film thickness calculated using the procedure described in [20].

Two viscoelastic uniaxial simulations (one simulation incorporating this factor) were performed to investigate the effect of the geometry factor on the deformation of the sample. Figure 7 shows the predicted radial and axial strain of the sample under a constant stress of 400 kPa. It can be seen from this figure that for a given axial strain, the radial strain in the simulation including the geometry factor is higher than in the simulation excluding the geometry factor. This is because the aspect ratio of bitumen films in tension decrease during the simulation causing a reduction in stiffness resulting in higher levels of radial strain. This geometric factor is included in all further viscoelastic simulations presented in this paper.

6.2 Uniaxial simulation

The objective of this sub-section is to investigate the deformation and dilation of sand asphalt under simulated uniaxial tests. To decrease the computation time, a sample of 16.5 mm in diameter and 33 mm in height, containing 1,000 particles was used in this simulation. A high contact bond strength was applied to all contacts to prevent bond breakage. The model parameters are detailed in Table 1 and were chosen to give sensible levels of axial strain and a similar shape creep curve compared to previously gathered experimental data [17]. It should be noted that the contact properties given in Table 1 relate to the stiffnesses between sand particles separated by bitumen. Previous researchers [21,22] have shown that the stiffnesses of pure bitumen in tension and in shear are expected to be related by the factor of 3 in the linear region

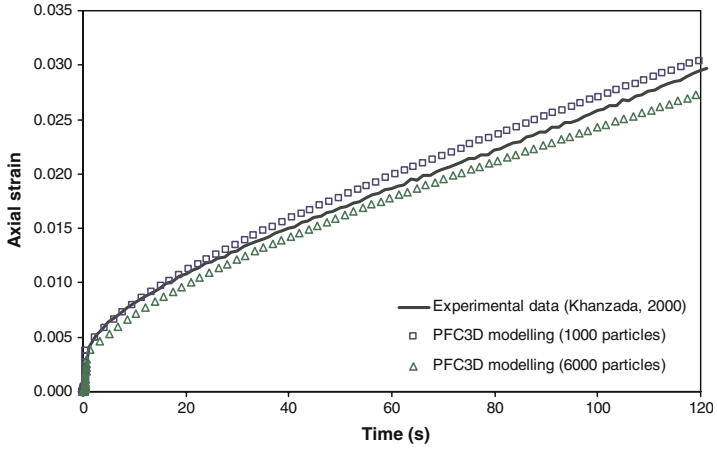

Fig. 8 Predicted and measured [17] axial strain for uniaxial creep test at 400 kPa as a function of time

of behaviour. Hence, the value of shear contact stiffness in Table 1 is taken to be one third of the value of normal tensile contact stiffness.

Figure 8 shows the predicted axial strain plotted as a function of loading time for an axial stress of 400 kPa. It can be seen from this figure that, as expected for this type of contact model, the strain response is a function of loading time comprising elastic, delayed elastic and viscous components. The measured curve is also shown in Figure 8 from where it can be seen that the predicted and measured curves are similar in magnitude and shape demonstrating the applicability of this approach.

Previous research has shown that at least 4,500 particles are required for the bulk elastic material properties (e.g. Young's modulus) calculated from a DEM simulation to be within 2% of the values calculated using a much larger number of particles (see Collop et al. [16] for further details). To investigate whether this effect is similar in a viscoelastic simulation, results from a sample containing 6,000 particles were used for comparison with those from the sample containing 1,000 particles. Also shown in Figure 8 is the plot of predicted axial strain as a function of time for the sample containing 6,000 particles. It can be seen from this figure that at a particular loading time, the axial strain calculated from the sample containing 1,000 particles is higher than the axial strain calculated from the sample containing 6,000 particles. For example, at a loading time of 100 s the sample containing 1,000 particles results in an over-prediction of approximately 12% compared to sample containing 6,000 particles which is consistent with previous results from the elastic simulations [16]. It should be noted that for practical reasons (computation time), results presented in the rest of this paper are based on samples containing 1,000 particles which will result in an over-prediction of the axial strain.

Figure 9 shows a plot of the simulated volumetric strain versus distortional strain. It can be seen from this figure that early in the test at distortional strain levels less than approximately 0.3% the volumetric strain is negative indicating compaction of the material. The volumetric strain then increases

Table 1 Burger's contact model parameters for viscoelastic simulations

Shear contact		Tension contact		Compression contact	
Property	Value	Property	Value	Property	Value
K_o^{s} (MN/m)	0.12	K_o^{n} (MN/m)	0.36	E_o^{n} (MN/m)	0.70
C_∞^{s} (MNs/m)	0.80	C_∞^{n} (MNs/m)	2.40		
K_1^{s} (MN/m)	0.03	K_1^{n} (MN/m)	0.09		
C_1^{s} (MNs/m)	0.80	C_1^{n} (MNs/m)	2.40		

approximately in proportion to the distortional strain as the material dilates, i.e.:

$$\dot{H} = s\left|\dot{E}\right|. \tag{4}$$

The parameter s can be interpreted as the steady-state dilation gradient which can be directly compared to the dilation gradient introduced earlier in the elastic simulations. For the case shown in Figure 9 the dilation gradient is approximately 0.8 (i.e. $s = 0.8$). Experimental data for the same idealised mixture tested at 20°C taken from Deshpande [23] is shown in Figure 9 for comparison. It can be seen by comparing the measured with the predicted data that, although the general shapes of the curves are similar, the measured dilation gradient is slightly higher and the simulation tends to over-predict the initial compaction phase at the beginning of the test. The reason for this not known but may relate to the fact that single sized particles have been used in the simulations whereas particles between 1.18 and 2.36 mm were used in the experiments. The under-prediction of the dilation gradient is likely to be because the particles in the numerical sample are perfectly spherical whilst in reality the sand particles are more angular, resulting in greater dilation. From the data shown in Figure 4 it can be concluded that the maximum dilation gradient for perfectly spherical particles under uniaxial stress conditions is approximately 0.8. To increase the dilation gradient further, more complex particle shapes are required which is beyond the scope of this paper.

Since an elastic compressive contact stiffness and a viscoelastic shear and tensile contact stiffness have been used, the ratio of compressive to tensile contact stiffness will increase during the simulation and, by analogy, to the results from the elastic simulation, it is likely that the dilation gradient will also change during the simulation. This can be seen from careful inspection of the data shown in Figure 9 where the slope is not constant and is shown in Figure 4 where the dilation gradient is plotted as a function of the ratio of compressive to tensile normal contact stiffness calculated from equation (2). It can clearly be seen from this figure that, as with the elastic case, the dilation gradient tends to increase as the ratio of compressive to tensile normal contact stiffness increases during the simulation. Also shown in Figure 9 is the result from a simulation undertaken using a sample containing 6,000 particles. It can be seen from this figure that the result from the simulation undertaken using 1,000 particles tends to slightly over-predict the volumetric strain at a given level of distortional strain although it should be noted that the effect is smaller than for the axial strain (see Figure 8).

6.3 Triaxial simulations

Previous experimental studies have shown that the dilation gradient of the sand asphalt is a function of the ratio of mean stress to deviator stress in a triaxial test [17,24]. The objective in this section is to investigate whether DEM can predict this. In triaxial tests, the deviatoric load Q and the cell pressure P are related to the principle stresses by:

$$\sum_{33} = \frac{Q}{A} + P,$$
$$\sum_{11} = \sum_{22} = P, \tag{5}$$

where A is the cross-sectional area of the specimen. Thus, the mean stress $\sum_{\mathrm{m}}$ and the deviator stress $\sum$ are given by:

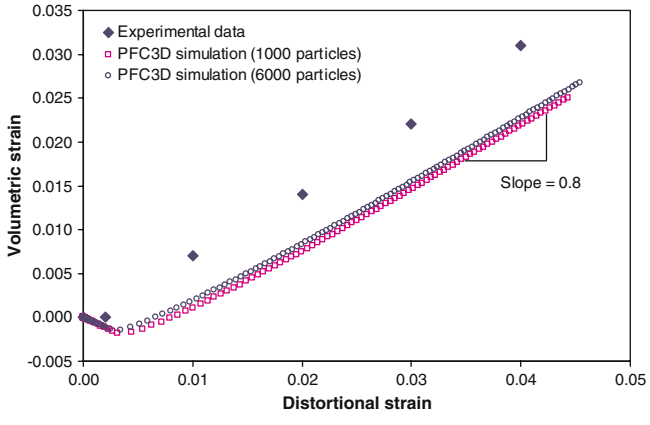

Fig. 9 Predicted and measured volumetric strain and distortional strain for uniaxial creep test at 400 kPa

$$\sum_{\mathrm{m}} = \frac{\sum_{kk}}{3} = P + \frac{Q}{3A},$$
$$\sum = \sum_{33} - \sum_{11} = \frac{Q}{A}. \tag{6}$$

The stress ratio, η is defined as the ratio of the mean stress to the deviator stress (i.e. $\eta = \sum_{\mathrm{m}} / \sum$). Figure 10 shows experimental data taken from Khanzada [17] where volumetric strain is plotted against distortional strain for deviator stresses of 400 and 1,000 kPa at stress ratios of 0.6 and 0.8. It can be seen from this figure that the dilation gradients from the tests with a stress ratio of 0.6 are higher than the dilation gradients from the tests with a stress ratio of 0.8.

A series of triaxial simulations were performed to investigate the effect of stress ratio and deviator stress on the predicted dilation gradient of the sand asphalt mixture. The sample preparation procedure was the same as that for the uniaxial simulations with the exception that the cylindrical boundary was not removed but was used to provide lateral confinement to the sample. To decrease the computation time, a sample 16.5 mm in diameter and 33 mm in height, containing 1,000 particles (1.8 mm in diameter) was used in the simulation. A high contact bond strength was applied to all contacts to prevent bond breakage. The same model parameters were used as in the unaxial viscoelastic simulations (see Table 1).

6.4 Effect of stress ratio

Figure 11 shows the predicted axial creep strain plotted as a function of time for a deviator stress of 400 kPa and stress ratio of 0.6. An experimental result obtained for a similar idealised asphalt mixture tested at the same deviator stress and stress ratio (taken from Khanzada [17]) is also shown in this figure. It can be seen that agreement is reasonable although the DEM tends to over-predict the steady-state dilation gradient although it should be noted that, as discussed earlier, the effect of using 1,000 particles will be to over-predict the axial strain response.

Three triaxial simulations were performed at a deviator stress of 400 kPa with stress ratios of 0.33 (uniaxial), 0.6 and 0.8. Figure 12 shows the predicted volumetric strain plotted against the distortional strain. It can be seen from this figure that as the stress ratio is increased the dilation gradient reduces. The dilation gradients calculated between distortional strain levels of 0.3 and 0.35% are plotted in Fig. 13. It can be seen from this figure that the predicted dilation gradient decreases from 0.8 at a stress ratio of 0.33 (uniaxial conditions) to 0.6 at stress ratio of 0.8. This indicates that the dilation gradient is lower at higher stress ratios, which is in agreement with the data shown in Figure 10 (which is also shown in Figure 13). This is because at a higher stress ratio, the confining stress is higher under a same level of deviator stress, resulting in less dilative (more contractive) volumetric strains.

A series of triaxial simulations was also performed at deviator stresses ranging from 100 to 800 kPa, with confining stress varied so that the stress ratio remained at 0.6 in all cases.

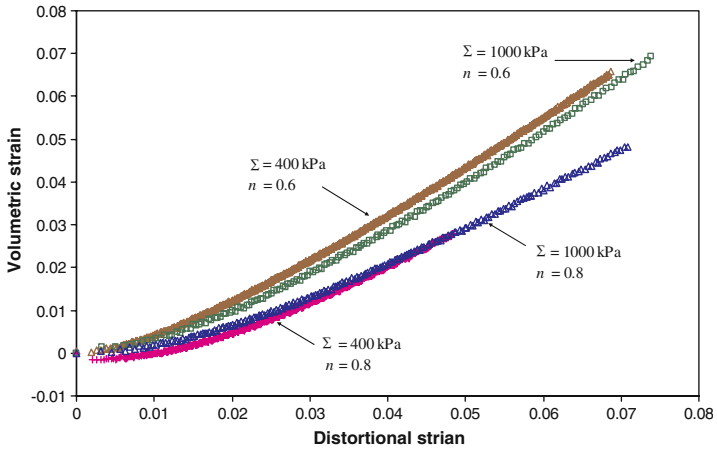

Fig. 10 Measured volumetric strain and distortional strain at different deviator stresses $\sum$ and stress ratios η (reproduced from [17]

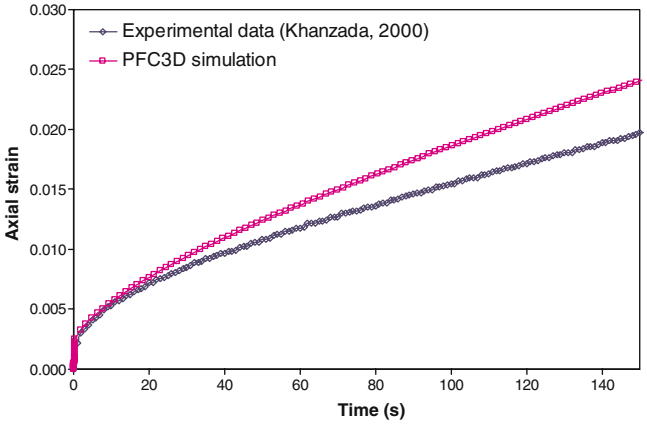

Fig. 11 Predicted and measured [17] axial strain as a function of time at a deviator stress of 400 kPa and stress ratio of 0.6

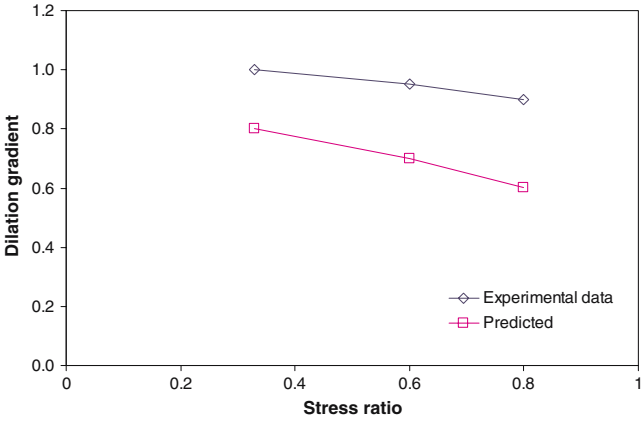

Fig. 13 The measured and predicted "steady state" dilation gradients at stress ratios η of 0.33, 0.6 and 0.8 for a deviatoric stress of 400 kPa

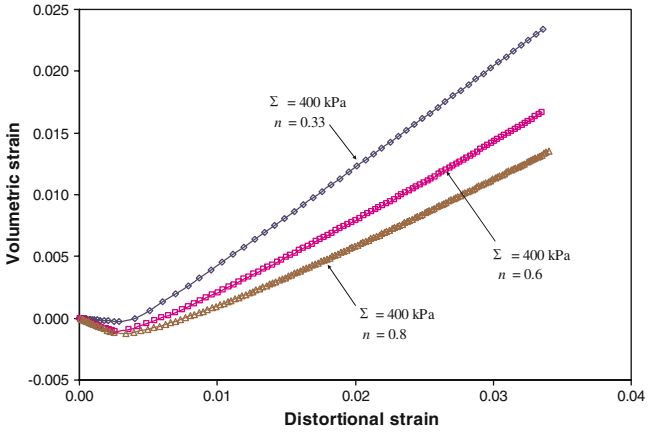

Fig. 12 The predicted volumetric strain and distortional strain at deviator stress $\sum$ of 400 kPa and stress ratios η of 0.33, 0.6 and 0.8

The same numerical sample as in the previous section was used. Figure 14 shows the predicted volumetric strain plotted against the deviator strain. It can be seen from this figure that approximately the same dilation gradients are observed for different deviator stresses indicating that the dilation gradient is only dependent on the stress ratio.

7 Summary and conclusions

- DEM has been used to simulate the behaviour of idealised asphalt mixtures under uniaxial and triaxial compressive creep loading.
- A numerical sample preparation procedure has been developed to ensure that the numerical specimen is initially isotropic and has the correct volumetrics.
- Elastic contact properties have been used to investigate the effect of the values of the shear and normal contact stiffnesses on bulk material properties (Young's modulus, bulk modulus and Poisson's ratio).
- The bulk modulus has been found to be linearly dependent on the normal contact stiffness and independent of the shear contact stiffness.
- Poisson's ratio has been found to be dependent only on the ratio of the shear contact stiffness to the normal contact stiffness.
- Elastic contact properties have been used to investigate the effect of the ratio of the compressive to tensile normal contact stiffnesses on the level of dilation. The dilation level in uniaxial test was found to be increases as the

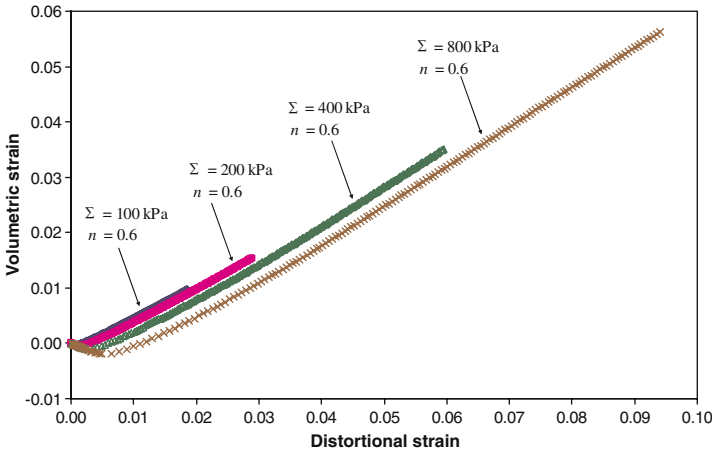

Fig. 14 Predicted volumetric strain and distortional strain at a stress ratio η of 0.6 for different deviator stress levels

ratio of compressive to tensile normal contact stiffness increases.

- A simple viscoelastic Burger's model was introduced to give time-dependent shear and normal tensile contact stiffnesses, whilst the normal compressive contact stiffness has been assumed to be elastic to represent aggregate to aggregate contact.
- The effect of changing bitumen film geometry on contact stiffnesses has been included in the viscoelastic simulations.
- The dilation gradient under uniaxial conditions was found to increase with time as the ratio of compressive to tensile contact stiffness increase as a function of time in the viscoelastic simulations.
- The model has been used to simulate axial strains and dilation gradients of an idealised sand asphalt and compared with experimental data.
- The dilation gradients from triaxial tests were found to be dependent only on stress ratio. The dilation gradient was found to increase as the stress ratio decreases.
- Future work will concentrate on correctly modelling particle shape using clump logic, in order to achieve even better agreement between the DEM and experimental data. It will then be possible to investigate the effect of particle size distribution on asphalt performance.

Acknowledgements The authors are grateful to the Nottingham Asphalt Research Consortium (NARC) for providing funding for this research.

References

1. Brown, S.F., Cooper, K.E.: A fundamental study of the stress–strain characteristics of a bituminous material. Asphalt Paving Technol **49**, 476 (1980)
2. Hopman, P.C., Valkering, C.P., Van der Heide, J.P.J.: Mixes and five design procedures: search for a performance related mix design procedure. Asphalt Paving Technol **61**, 188 (1992)
3. Sousa, J.B., Deacon, J.A., Monismith, C.L.: Effect of laboratory compaction method on permanent deformation characteristics of asphalt-aggregate mixtures. Asphalt Paving Technol **60**, 533 (1991)
4. Harvey, J., Monismith, C.L., Sousa, J.B.: An investigation of field and laboratory compacted asphalt-rubber, SMA, recycled and conventional asphalt-concrete mixes using SHRP project A-003A equipment. Asphalt Paving Technol **63**, 511 (1994)
5. Renken, P.: Influence of specimen preparation onto the mechanical behaviour of asphalt aggregate mixtures. In: Proceedings of the 2nd Eurasphalt and Eurobitume Congress, p. 729 (2000)
6. Tashman, L., Masad, E., Peterson, B., Saleh, H.: Internal structure analysis of asphalt mixes to improve the simulation of Superpave gyratory compaction to field compaction. Asphalt Paving Technol **70** (2001)
7. Collop, A.C., Scarpas, A., Kasbergen, C., de Bondt, A.: Development and finite element implementation of a stress dependent elasto-visco-plastic constitutive model with damage for asphalt. Transport Res Rec (in press) (2004)
8. Cundall, P.A., Strack, O.D.L.: A discrete numerical model for granular assemblies. Géotechnique **29**(1), 47 (1979)
9. Itasca Consulting Group Inc.: Particle flow code in three dimensions (1999)
10. Robertson, D.: Numerical simulations of crushable aggregates. PhD dissertation, University of Cambridge (2000)
11. McDowell, G.R., Harireche, O.: Discrete element modelling of yielding and normal compression of sand. Geotechnique **52**(4), 299 (2002)
12. McDowell, G.R., Harireche, O.: Discrete element modelling of soil particle fracture. Geotechnique **52**(2), 131 (2002)
13. Ullidtz, P.: Analytical tools for design of flexible pavements. Keynote Address. In: Proceedings if the 9th International Conference on Asphalt Pavements, Copenhagen, issue 3, 22 (2003)
14. Rothenburg, L., Bogobowicz, A., Haas, R., Jung, F., Kennepohl, G.: Micromechanical modelling of asphalt concrete in connection with pavement rutting problems. In: Proceedings of the 7th International Conference on Asphalt Pavements, Nottingham, issue 1, 230 (1992)
15. Buttlar, W.G., You, Z.: Discrete element modelling of asphalt concrete: a microfabric approach. J Transport Bd Nat Res Council Wash DC **1757**, 111 (2001)
16. Collop, A.C., McDowell, G.R., Lee, Y.: Modelling the behaviour of idealised asphalt mixture using the distinct element method. In: Presented at the 83rd Annual Meeting of the Transportation Research Board, Washington DC (2004)
17. Khanzada, S.: Permanent deformation in bituminous mixtures. PhD Thesis, University of Nottingham (2000)
18. Cheung, C.Y.: Mechanical behaviour of bitumens and bituminous mixes. PhD Thesis, University of Cambridge (1995)

19. Harvey, J.A.F.: Bitumen films in tension. PhD Thesis, University of Cambridge (2000)
20. Read, J.M., Whiteoak, C.D.: The shell bitumen handbook, 5th edn. London: Thomas Telford Publishing 2003
21. Cheung, C.Y., Cebon, D.: Experiment study of pure bitumen in tension, compression and shear. J Rheol **41**(1), 45 (1997)
22. Lethersich, W.: The mechanical behaviour of bitumen. J Soc Chem Indus. Transact Commun **61**, 101 (1942)
23. Deshpande, V.S.: Steady-state deformation behaviour of bituminous mixes. PhD Thesis, University of Cambridge (1997)
24. Huang, Y.H.: Deformation and volume change characteristics of a sand asphalt mixture under constant direct triaxial compressive stresses. Highway Res Rec **178**, 60 (1967)